3-17-2010

High-Spatial and High-Mass Resolution Imaging of Surface Metabolites of Arabidopsis thaliana by Laser Desorption-Ionization Mass Spectrometry Using Colloidal Silver

Ji Hyun Jun
Iowa State University, jhjun84@gmail.com

Zhihong Song
Iowa State University

Zhenjiu Liu
Iowa State University

Basil Nikolau
Iowa State University, dimmas@iastate.edu

Edward S. Yeung
Iowa State University, yeung@ameslab.gov

See next page for additional authors

High-Spatial and High-Mass Resolution Imaging of Surface Metabolites of Arabidopsis thaliana by Laser Desorption-Ionization Mass Spectrometry Using Colloidal Silver

Abstract

High-spatial resolution and high-mass resolution techniques are developed and adopted for the mass spectrometric imaging of epicuticular lipids on the surface of *Arabidopsis thaliana*. Single cell level spatial resolution of ~12 μm was achieved by reducing the laser beam size by using an optical fiber with 25 μm core diameter in a vacuum matrix-assisted laser desorption ionization-linear ion trap (vMALDI-LTQ) mass spectrometer and improved matrix application using an oscillating capillary nebulizer. Fine chemical images of a whole flower were visualized in this high spatial resolution showing substructure of an anther and single pollen grains at the stigma and anthers. The LTQ-Orbitrap with a MALDI ion source was adopted to achieve MS imaging in high mass resolution. Specifically, isobaric silver ion adducts of C29 alkane (m/z 515.3741) and C28 aldehyde (m/z 515.3377), indistinguishable in low-resolution LTQ, can now be clearly distinguished and their chemical images could be separately constructed. In the application to roots, the high spatial resolution allowed molecular MS imaging of secondary roots and the high mass resolution allowed direct identification of lipid metabolites on root surfaces.

Disciplines

Analytical Chemistry | Chemistry

Comments

Reprinted (adapted) with permission from *Analytical Chemistry* 82 (2010): 3255, doi: 10.1021/ac902990p.

Authors

Ji Hyun Jun, Zhihong Song, Zhenjiu Liu, Basil Nikolau, Edward S. Yeung, and Young Jin Lee

Anal. Chem. **2010,** *82,* 3255–3265

High-Spatial and High-Mass Resolution Imaging of Surface Metabolites of *Arabidopsis thaliana* by Laser Desorption-Ionization Mass Spectrometry Using Colloidal Silver

Ji Hyun Jun,[†,‡] Zhihong Song,[†,§] Zhenjiu Liu,[†] Basil J. Nikolau,[†,§] Edward S. Yeung,[†,‡] and Young Jin Lee*[,†,‡]

Ames Laboratory, U.S. Department of Energy, Ames, Iowa 50011, and Department of Chemistry and Department of Biochemistry, Biophysics, and Molecular Biology, Iowa State University, Ames, Iowa 50011

High-spatial resolution and high-mass resolution techniques are developed and adopted for the mass spectrometric imaging of epicuticular lipids on the surface of *Arabidopsis thaliana*. Single cell level spatial resolution of ~12 μm was achieved by reducing the laser beam size by using an optical fiber with 25 μm core diameter in a vacuum matrix-assisted laser desorption ionization-linear ion trap (vMALDI-LTQ) mass spectrometer and improved matrix application using an oscillating capillary nebulizer. Fine chemical images of a whole flower were visualized in this high spatial resolution showing substructure of an anther and single pollen grains at the stigma and anthers. The LTQ-Orbitrap with a MALDI ion source was adopted to achieve MS imaging in high mass resolution. Specifically, isobaric silver ion adducts of C29 alkane (*m/z* 515.3741) and C28 aldehyde (*m/z* 515.3377), indistinguishable in low-resolution LTQ, can now be clearly distinguished and their chemical images could be separately constructed. In the application to roots, the high spatial resolution allowed molecular MS imaging of secondary roots and the high mass resolution allowed direct identification of lipid metabolites on root surfaces.

Mass spectrometric imaging of biological tissues can provide the spatial distribution of analytes and their abundances, unveiling the underlying molecular biology in unprecedented details.[1−7] Although ion beam radiation provides submicrometer spatial resolution for subsequent mass spectrometric analysis, the energetic ion beams often produce extensive fragmentation and limits the sensitivity of detecting molecular species.[8] On the other hand, liquid or gas stream based sampling, probably the softest types of desorption ionization, have limitations in controlling the stream beam size below the ~100 μm scale.[9] For these reasons, laser interrogation of sample tissues is expected to be the best choice for molecular imaging at the micrometer size level.

Addition of a matrix is a common procedure to mediate laser energy absorption and to ionize biomolecules without fragmentation.[10] The size of matrix crystals formed by traditional organic acid matrixes have been obstacles for mass spectrometry (MS) imaging,[11] and peaks associated with matrix ions have inhibited the MS imaging of small metabolites.[12] Possible solutions include the use of water as a matrix in infrared laser ablation and/or ionization[13] and the use of colloidal silver[6] or graphite as a matrix.[14] The use of colloidal silver is of particular interest in the analysis of epicuticular lipid metabolites on plant surface for several reasons. Most important of these is the fact that this material does not crystallize and forms a homogeneous layer, thus providing a homogeneous matrix.[6] Another attribute of this choice is that silver ions form adducts with nonpolar or partially polar lipid molecules. Silver ions have been used as a cationizing reagent for hydrocarbons.[15,16]

There have been many efforts to reduce the laser spot size in MALDI imaging such as the use of a pinhole[1] or utilizing multiple focusing lenses.[17] Recently, Caprioli's group achieved high spatial resolution MS images of 4.8 μm size on a mouse brain tissue[18]

* To whom correspondence should be addressed. E-mail: yjlee@iastate.edu.
† Ames Laboratory, U.S. Department of Energy.
‡ Department of Chemistry, Iowa State University.
§ Department of Biochemistry, Biophysics, and Molecular Biology, Iowa State University.

(1) Caprioli, R. M.; Farmer, T. B.; Gile, J. *Anal. Chem.* **1997**, *69*, 4751–4760.
(2) Reyzer, M. L.; Hsieh, Y.; Ng, K.; Korfmacher, W. A.; Caprioli, R. M. *J. Mass Spectrom.* **2003**, *38*, 1081–1092.
(3) Stoeckli, M.; Chaurand, P.; Hallahan, D. E.; Caprioli, R. M. *Nat. Med.* **2001**, *7*, 493–496.
(4) Stoeckli, M.; Staab, D.; Staufenbiel, M.; Wiederhold, K. H.; Signor, L. *Anal. Biochem.* **2002**, *311*, 33–39.
(5) Rohner, T. C.; Staab, D.; Stoeckli, M. *Mech. Ageing Dev.* **2005**, *126*, 177–185.
(6) Cha, S.; Song, Z.; Nikolau, B. J.; Yeung, E. S. *Anal. Chem.* **2009**, *81*, 2991–3000.
(7) Burrell, M.; Earnshaw, C.; Clench, M. *J. Exp. Bot.* **2007**, *58*, 757–763.
(8) Ostrowski, S. G.; Szakal, C.; Kozole, J.; Roddy, T. P.; Xu, J.; Ewing, A. G.; Winograd, N. *Anal. Chem.* **2005**, *77*, 6190–6196.
(9) Ifa, D. R.; Manicke, N. E.; Dill, A. L.; Cooks, R. G. *Science* **2008**, *321*, 805.
(10) Ute Bahr, A. D.; Karas, M.; Hillenkanp, F.; Giessmann, U. *Anal. Chem.* **1992**, *64*, 2866–2869.
(11) Altelaar, A. F.; van Minnen, J.; Jimenez, C. R.; Heeren, R. M.; Piersma, S. R. *Anal. Chem.* **2005**, *77*, 735–741.
(12) Guo, Z.; Zhang, Q.; Zou, H.; Guo, B.; Ni, J. *Anal. Chem.* **2002**, *74*, 1637–1641.
(13) Li, Y.; Shrestha, B.; Vertes, A. *Anal. Chem.* **2007**, *79*, 523–532.
(14) Cha, S.; Zhang, H.; Ilarslan, H. I.; Wurtele, E. S.; Brachova, L.; Nikolau, B. J.; Yeung, E. S. *Plant J.* **2008**, *55*, 348–360.
(15) Kahr, M. S.; Wilkins, C. L. *J. Am. Soc. Mass Spectrom.* **1993**, *4*, 453–460.
(16) Dutta, T. K.; Harayama, S. *Anal. Chem.* **2001**, *73*, 864–869.
(17) Spengler, B.; Hubert, M. *J. Am. Soc. Mass Spectrom.* **2002**, *13*, 735–748.
(18) Chaurand, P.; Angel, P. M.; Caprioli, R. M. *Proceedings of the 57th ASMS Conference on Mass Spectrometry and Allied Topics*, Philadelphia, PA, May 31−June 4, 2009; oral session MOAam10:10.

10.1021/ac902990p
Published on Web 03/17/2010

using coaxial laser illumination.[19] Hölscher and co-workers reported single cell level, ~10 μm size, MS imaging of plant materials using the smartbeam technology in the Ultraflex III time-of-flight (TOF) mass spectrometer.[20] Without matrix, they could get images of UV-absorbing secondary metabolites in plant tissues. Limiting the beam size through an optical fiber could be an easy way to improve resolution; however, its application has been limited only to crystalline structures of standard samples plated on a MALDI target.[21] Vertes' group acquired single cell mass spectra of plant materials using an etched tip of an optical fiber with a resolution down to 30−40 μm in laser-ablation electrospray ionization,[22] but its application to MS imaging has not been reported yet. Previously, we reported the use of colloidal silver to characterize the distribution of epicuticular lipid metabolites on the surfaces of a number of plant organs with a laser beam size of ~100 μm diameter.[6] In the present work, we report single cell level spatial resolution with a laser spot size of ~12 μm using an optical fiber with a 25 μm core diameter and applied that to the MS imaging of *Arabidopsis* flowers and roots.

High mass resolution is another very important issue in MS imaging.[23] Unlike typical metabolomic analysis with gas chromatography/mass spectrometry (GC/MS) or liquid chromatography/mass spectrometry (LC/MS), the lack of chromatographic separation makes it vulnerable to false analyte assignments. To minimize the problem, we typically perform GC/MS analysis of the surface extracted lipid metabolites in parallel to MS imaging. However, even this strategy is limited for several reasons. First, identification of novel metabolites is dependent on authentication via an alternative identification strategy. Second, when two isobaric molecules occur in the sample, one cannot correlate the two analytes. Third, the relationship between sampling depth in MALDI imaging and chemical extraction for GC/MS is unknown. Tandem mass spectrometry (MS/MS) imaging (often called imaging mass spectrometry/mass spectrometry (IMS/MS)) could be a solution for differentiating isobaric ions but only if each isobaric compound has well-known characteristic fragmentation ions.[24] High-resolution mass spectrometry offers solutions to most of these issues. High-resolution MS can separate isobaric ions based on their slight mass differences. Moreover, it can directly determine the chemical compositions of unknown metabolites. The utility of the high-resolution LTQ-Orbitrap mass spectrometer in imaging MS has been recently reported by Landgraf and co-workers in an application to rat brain spinal cord tissues.[25] Here, we demonstrate an application of MALDI LTQ-Orbitrap to plant materials, especially the discrimination of notorious isobaric epicuticular lipids, alkanes, and aldehydes, and the direct identification of metabolites on the tissue surfaces.

EXPERIMENTAL SECTION

Chemicals. Colloidal silver (99.99% pure silver, 0.65 nm; 20 ppm) was purchased from Purest Colloids, Inc. (Westampton, NJ). Colloidal graphite aerosol spray was obtained from Alfa Aesar (Ward Hill, MA). 2-Propanol (HPLC grade) was purchased from Fisher Scientific (Fairlawn, NJ). *N*,*O*-Bis(trimethylsilyl)trifluoroacetamide with trimethylchlorosilane (BSTFA/TMCS), Murashige and Skoog basal salt mixture, and standard compound docosane were obtained from Sigma-Aldrich (St. Louis, MO).

Plant Growth Conditions. *Arabidopsis thaliana* ecotype Landsberg *erecta* (Ler-0) and *eceriferum* mutant (*cer*1, genetic stock CS31) were obtained from the *Arabidopsis* Biological Resource Center (Columbus, OH, US). Seeds were sterilized and sown on Murashige and Skoog basal salt mixture (MS) media in Petri dishes. The dishes were placed in the growth room for 10 days after breaking seed dormancy by maintaining them at 4 °C for 4 days. On the 15th day, the seedlings were transferred to soil in 5 cm × 5 cm pots for continuous growth. Flower and root samples for imaging were collected on the 42nd day and the 46th day, respectively. The stems used for the differentiation of isobaric ions with high-resolution mass spectrometry and the depth-profiling experiments were 38 and 29 days old, respectively. The growth room was set at 24 °C with continuous illumination at 85 $\mu E\ m^{-2}\ s^{-1}$ and ambient relative humidity. For the identification of root surface metabolites by GC/MS and LTQ-Orbitrap, seeds were sterilized and cultured in liquid media for 16 and 21 days, respectively, at room temperature with continuous shaking at 100 rpm in 500 mL flasks containing 250 mL of MS media.

Sample Preparation for LDI MS Imaging. Each plant organ dissected from the intact plants was immediately attached onto a stainless steel plate using a conductive double-sided tape (3M; St. Paul, MN). Avoiding physical contacts on the targeted areas and using a stream of nitrogen gas to assist sample attachment minimized physical damage on the sample tissues. The attached samples were dried under a moderate vacuum (~50 Torr) for 30−60 min to minimize metabolite turnover.

A commercial airbrush (Aztek A470; Testor; Rockford, IL) was modified to become an oscillating spray device[26] by replacing the inner spraying tip with a fused silica capillary (100 μm i.d., 360 μm o.d.; Polymicro Technology; Phoenix, AZ) for homogeneous matrix application. Matrixes were delivered to the modified airbrush through a syringe pump (Fisher Scientific; Pittsburgh, PA) and sprayed onto plant tissues by nebulizing with N_2 gas at a pressure of 40 psi. The distance between the tip of the capillary and the sample plate was kept at 9 cm. The matrix flow rate was set at 50 $\mu L\ min^{-1}$ and spraying volumes were 0.15 and 0.3 mL for colloidal silver and colloidal graphite, respectively. The matrix was applied by spraying for 12 s increments, interrupted by 30 s intervals to allow for vaporization of the solvent and thus reducing aggregation of the matrix droplets.

Sample Preparation for Gas Chromatography/Mass Spectrometry. Root samples from liquid MS media were collected on the 16th day and weighed. An aliquot of internal standard (docosane) was added to the root surface. Surface lipids were extracted by completely immersing the roots in chloroform for

(19) Chaurand, P.; Schriver, K. E.; Caprioli, R. M. *J. Mass Spectrom.* **2007**, *42*, 476–489.
(20) Holscher, D.; Shroff, R.; Knop, K.; Gottschaldt, M.; Crecelius, A.; Schneider, B.; Heckel, D. G.; Schubert, U. S.; Svatos, A. *Plant J.* **2009**, *60*, 907–918.
(21) Qiao, H.; Piyadasa, G.; Spicer, V.; Ens, W. *Int. J. Mass Spectrom.* **2009**, *281*, 41–51.
(22) Shrestha, B.; Vertes, A. *Anal. Chem.* **2009**, *81*, 8265–8271.
(23) Taban, I. M.; Altelaar, A. F.; van der Burgt, Y. E.; McDonnell, L. A.; Heeren, R. M.; Fuchser, J.; Baykut, G. *J. Am. Soc. Mass Spectrom.* **2007**, *18*, 145–151.
(24) Cha, S.; Yeung, E. S. *Anal. Chem.* **2007**, *79*, 2373–2385.
(25) Landgraf, R. R.; Prieto Conaway, M. C.; Garrett, T. J.; Stacpoole, P. W.; Yost, R. A. *Anal. Chem.* **2009**, *81*, 8488–8495.
(26) Chen, Y. F.; Allegood, J.; Liu, Y.; Wang, E.; Cachon-Gonzalez, B.; Cox, T. M.; Merrill, A. H.; Sullards, M. C. *Anal. Chem.* **2008**, *80*, 2780–2788.

60 s and then dried under nitrogen gas. Samples were derivatized using BSTFA/TCMS (65 °C, 30 min) for GC/MS analysis.

Mass Spectrometry Imaging. High spatial resolution MS images were acquired with a linear ion trap mass spectrometer with a MALDI ion source (vMALDI LTQ; Thermo Electron; San Jose, CA).[27] For the vMALDI LTQ, the N_2 laser system from Spectral Physics was used with a maximum energy of 280 μJ/pulse and maximum frequency of 20 Hz. The laser beam was transferred to the mass spectrometer through an optical fiber. The original optical fiber of 200 μm i.d. was replaced with a 25 μm core multimode optical fiber (Oz Optics; Ottawa, ON, Canada) to reduce the laser beam size. The laser spot size was ~12 μm after the refocusing lens, as measured from a burn mark test on a thin film of α-cyano-4-hydroxycinnamic acid coated on a stainless steel plate. The MALDI source pressure was kept at 170 mTorr.

A high-resolution mass spectrometer with a MALDI source (MALDI LTQ-Orbitrap Discovery; Thermo Electron) was also used for profiling and imaging.[27] It has a mass resolution of 30 000 at m/z 400 and a mass accuracy of 5 ppm with external calibration and 3 ppm with internal calibration. This system uses a N_2 laser (MNL 100; Lasertechnik Berlin; Berlin, Germany) with a maximum energy of 80 μJ/pulse and maximum repetition rate of 60 Hz. The laser was directly attached to the mass spectrometer and transferred the laser beam through mirrors and lenses without guidance by an optical fiber. The laser spot size was adjusted to 25 μm by placing a black-painted stainless steel plate with a pinhole aperture with a diameter of 3 mm directly in the laser beam path. The MALDI source pressure was maintained at 75−80 mTorr.

Data Acquisition and Processing for Mass Spectrometric Imaging. Data were acquired from plant tissues with a fixed number of laser shots without automatic gain control (AGC). The optimum number of laser shots and laser power were determined based on tests conducted with AGC turned-on, performed on a small area of a test sample. The sample plate was scanned with the raster size of 12 μm for high-spatial resolution imaging experiments with the vMALDI LTQ and 25 or 50 μm for high-mass resolution imaging experiments with MALDI LTQ-Orbitrap.

Mass spectrometric images were generated with a tissue imaging visualization software (ImageQuest 1.0.1; Thermo Finnigan). Ion signals of interest were normalized relative to the silver dimer peak intensity (m/z 216; $[^{107}Ag + {}^{109}Ag]^+$) on each mass spectrum, and the MS images were constructed with the mass window of ±0.5 and ±0.008 Da for LTQ and LTQ-Orbitrap data, respectively. Some data sets could not be properly displayed as MS images with ImageQuest. In these cases, ion signals were extracted for each position using a custom program from Thermo (vMALDIDataExtract) and MS images were generated using a homemade program written in Python (version 2.5; http://www.python.org/) with a Matplot library (http://matplotlib.sourceforge.net/).

Gas Chromatography/Mass Spectrometry. GC/MS analysis was performed with an Agilent 6890 gas chromatograph and 5973N mass spectrometer (Agilent Technologies; Palo Alto, CA). The HP-5 ms column (30 m × 0.25 mm i.d. coated with 0.25 μm thick (5%-phenyl)-methylpolysiloxane; Agilent Technologies) was temperature programmed from 80 to 320 at 5 °C min^{-1} with helium flow rate at 2.0 mL min^{-1}. Electron ionization was used with 70 eV electron energy. The GC/MS data files were deconvoluted by NIST AMDIS software and searched against an in-house mass spectral library and NIST05 spectral library.

RESULTS AND DISCUSSION

Laser Spot Size and Matrix Homogeneity. The vMALDI LTQ mass spectrometer utilizes an optical fiber to transfer the laser beam from the laser source to the MALDI ion source. Utilizing small core optical fibers and after careful realignment of the optical components, we could routinely reduce the laser spot size to about half the size of the optical fibers' core. Figure S-1 in the Supporting Information shows the laser burn marks of a size of 12−13 μm with a 25 μm optical fiber and ~6 μm with a 10 μm optical fiber.

The total laser output coming out of the optical fibers, however, decreases rapidly with the fiber size and as would be expected so does the subsequent ion signal. Hence, the laser power was increased at the beam source to maintain the comparable ion signal. For example, to maintain the ion signal at the level obtained with the 200 μm optical fiber, the laser beam power was increased from 3 to 5% to almost 100% when a 25 μm size optical fiber was used to reduce the laser spot size. Having maximized the laser beam power with a 25 μm size optical fiber, we rationalized that if ion yields are linearly proportional to the laser beam power, it may be possible to obtain equal quality LDI MS spectra even with a lower laser power by acquiring and integrating spectra from multiple laser shots, which would allow the use of optical fibers with even smaller diameters. This could be performed with an ion trap mass spectrometer by accumulating a sufficient number of ions in the trap before mass spectral data acquisition. Unfortunately, a minimum threshold laser power is required for surface analytes to acquire sufficient energy to be desorbed and ionized.[28] Beyond this minimum threshold of laser power, ion yield increases linearly with respect to photon influx until saturation.[28] Although we could observe laser burn marks on the matrix with multiple laser shots (Figure S-1 in the Supporting Information), we could not acquire sufficient analyte ions for reliable MS imaging with the optical fiber of 10 μm. Thus, the practical limit of spatial resolution is ~12 μm by using the optical fiber of 25 μm. In the future, a more powerful laser or a better way of coupling may allow further reduction in the beam size while maintaining useful signal levels. It should be noted that the sampling area is reduced as the square of the beam size and ion signals will be eventually limited by the available analytes, allowing MS imaging of only high-abundance molecules.

The homogeneous application of the matrix is another important requirement for high spatial resolution in MS imaging. We adopted colloidal silver as an additive for MS imaging of lipid metabolites on plant surfaces.[6] Figure 1a shows an SEM image of a bare stainless steel plate sprayed with colloidal silver using the commercial nebulizer used previously.[6] It shows that the surface is covered with randomly spread ~50 μm-size dark specks, which according to Auger spectroscopic analysis have a high

(27) Strupat, K.; Kovtoun, V.; Bui, H.; Viner, R.; Stafford, G.; Horning, S. *J. Am. Soc. Mass Spectrom.* **2009**, *20*, 1451–1463.

(28) Alcantara, J. F.; Vadillo, J. M.; Laserna, J. J. *Rapid Commun. Mass Spectrom.* **2008**, *22*, 1999–2005.

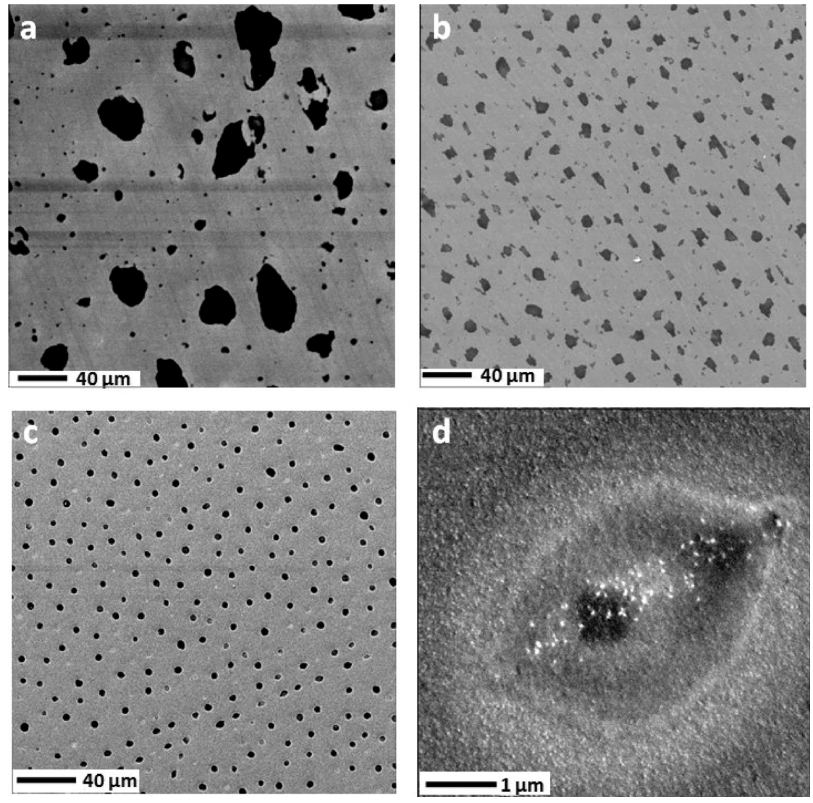

Figure 1. Homogeneity in matrix application: SEM images of bare stainless steel plates sprayed with colloidal silver using a commercial nebulizer (a) and oscillating capillary nebulizer without (b) or with (c) 4 times the volume of 2-propanol. Part d is a zoomed-in SEM image of one of the black specks shown in part c.

carbon content; presumably these originated from the organic additives that are added to the colloid preparations to minimize aggregation of the silver nanoparticles. To minimize this heterogeneity, the matrix was applied with a modified commercial airbrush, adopting oscillating capillary nebulizer developed by Sullards and co-workers.[26] Specifically, we replaced the original spray tip with a fused silica capillary with 100 μm i.d., which is connected to a syringe pump. The fused silica capillary is continuously oscillated by nebulizing gas flowing between the capillary and the outer tip, and this has the effect of reducing sizes of the droplets that are deposited on the surface. With this modification, sprayed droplets are almost invisible and the sizes of the organic, additive-derived black specks are much smaller, $\sim$10 μm (Figure 1b). The size of these specks could be further reduced to 3$-$5 μm by spraying the colloidal silver with the addition of four volumes of 2-propanol (Figure 1c). The inclusion of this organic solvent makes smaller droplets due to low surface tension and fast vaporization. Although the use of organic solvents for matrix dissolution in MALDI imaging has been suggested to have a potential problem of inducing redistribution of surface analytes,[26] here, the small droplet size would not invoke such an issue. Figure 1d shows a higher magnification image of a black speck shown in Figure 1c. White silver particles deposited on the surface have a size of $\sim$10 nm or smaller and were uniformly distributed on the outside of the speck, whereas those on the inside are somewhat aggregated toward the center. We speculate some silver particles get trapped by organic droplets and aggregate at the center as they are sprayed. Hence, our matrix homogeneity is limited by the size of the black specks, 3$-$5 μm when applied with 2-propanol or $\sim$10 μm when applied without 2-propanaol; in either case this is sufficient to provide a homogeneous matrix with the laser spot size used in the imaging experiments.

While the laser beam size and matrix homogeneity are the two most important factors that influence the spatial resolution in MALDI MS imaging, there also are other factors that need to be considered, including plate movement reproducibility and the actual area from which analytes are desorbed. Unfortunately, accurate assessment of the overall spatial resolution in MS imaging is hampered by the difficulty in preparing homogeneously spread analytes on surfaces at micrometer scales. Such an effort requires extensive surface study and is beyond the scope of the current research. Such a study would be valuable in the further development of the related research; however, in the current study we simply hypothesize other factors are relatively ignorable compared to the laser beam size and presume our spatial resolution is mostly dictated by the laser spot size of $\sim$12 μm. We have some evidence that partially support this hypothesis, i.e., plate movement reproducibility is less than 3 μm according to the manufacturer's specification; homogeneous LDI MS images were obtained for standard compounds with a larger laser beam size (data not shown).

MS Imaging of *Arabidopsis* Flowers at High Spatial Resolution. Figure 2 shows the chemical image of C29 alkane on an *Arabidopsis* flower monitored as the silver ion adduct obtained at a spatial resolution of 12 μm. We obtained "photo-quality" fine chemical images of surface lipid metabolites in this small area of only 4 $\times$ 3 mm^2. Such spatial resolution allows single cell level localization of the molecules, showing fine

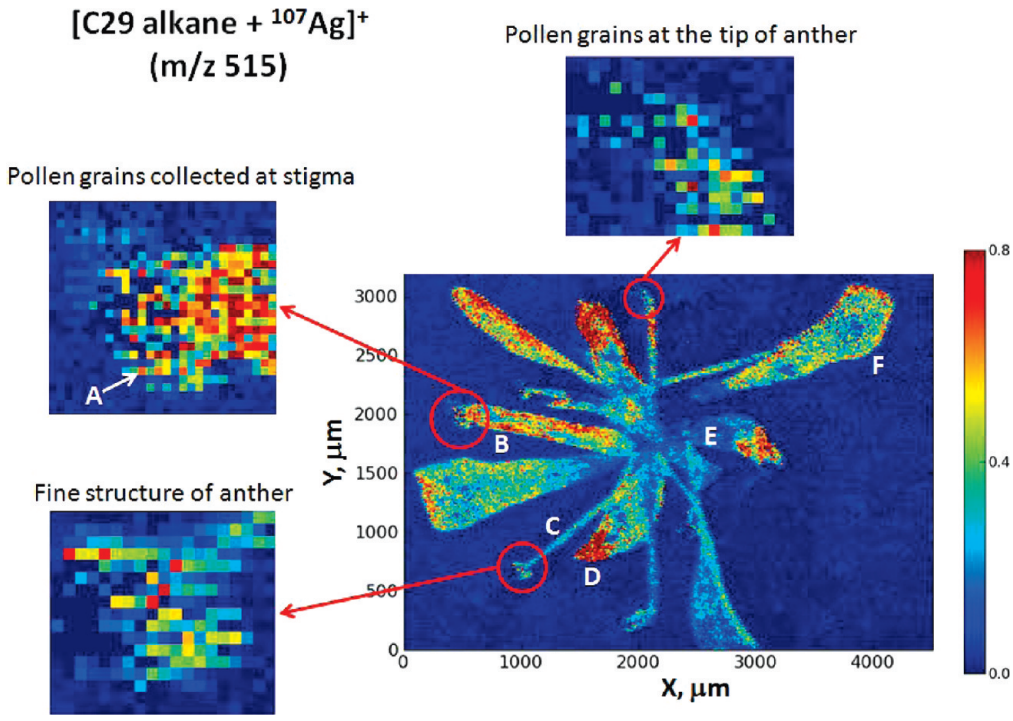

Figure 2. MS imaging in single cell level high spatial resolution demonstrated on an *Arabidopsis* flower. MS image of silver ion adduct of C29 alkane (*m*/*z* 515) on an *Arabidopsis* flower obtained with the spatial resolution of 12 μm (12 μm for both laser spot size and raster size). Ion abundances are normalized to the silver dimer, $[^{107}Ag + {}^{109}Ag]^+$ (*m*/*z* 216). Single cell level high spatial resolution is demonstrated in zoomed-in images of the stigma and anthers. The letters indicate the positions of single pixels for the mass spectra shown in Figure 3.

structures of an anther (tip of stamen) and single pollen grains at the stigma (tip of carpel) and anthers as shown in the zoomed-in images in Figure 2. We have several strong lines of evidence that those single pixels with high ion intensities around the stigma and anthers are pollen grains: (1) the size is equivalent to the known size of *Arabidopsis* pollens, ~10 μm; (2) they are seen only at the tip of stamens (male organ) and carpel (female organ), where pollens are supposed to be found; (3) we observed similar mass spectral patterns on each single pollen pixel (data not shown). These pollen grains probably fell to the MALDI plate and were scattered around the stigma and anthers in the process of sample preparation. Nakata and co-workers used the secondary ion mass spectrometry (SIMS) technique to obtain cross-sectional images of large size pollen particles (~100 μm), detecting mostly fragments such as PO_3^- or HPO_4^-.[29]

Figure 3 shows "single pixel" mass spectra derived from different tissues of the flower shown in Figure 2: single pollen grain, side of stamen filament, side of style (middle part of carpel), tip of sepal, middle of sepal, and side of petal. Table 1 shows a semiquantitative comparison of each lipid molecule shown in Figure 3 normalized to the silver dimer peak, $[^{107}Ag + {}^{109}Ag]^+$ (*m*/*z* 216). There are a few things to be noted. First of all, there is sufficient ion signal in each pixel whose dimensions correspond to only 12×12 μm^2. Ion signal levels are ~10^5 counts for the base peaks in all the spectra shown in Figure 3, implying that there are sufficient signals even if the sampling size is reduced to 2–5 μm. Second, the spectral patterns obtained from the individual tissues of the flower are quite different indicating unique metabolite distributions on each tissue. The pollen grain has a broad distribution of epicuticular lipid molecules (Figure 3A; Table 1). The carpel, in contrast, is rather unique in that C29 ketone is the most abundant surface lipid, showing more than 5-fold higher intensity than on the other tissues, while C29 alkane and C30 fatty acid are also the most abundant among the tissues (Figure 3B; Table 1). The high abundance of these three cuticular lipid metabolites is consistent with the fact that they are intermediates on the same metabolic pathway[30] (C30 fatty acid → (C30 aldehyde) → C29 alkane → C29 ketone), which suggests that fatty acid elongation to C30 fatty acid and the subsequent production of the downstream metabolites is unusually efficient in the epidermal cells of the carpel. Also in support of this hypothesis is the finding that carpels have the most abundant level of C30 alcohol, than on the other tissues, which is an alternative metabolic product of the C30 fatty acid. In contrast, at the tip of sepal (Figure 3D; Table 1), C29 alkane shows the second highest abundance, whereas C29 ketone abundance is the lowest. This may indicate that the conversion of C29 alkane to C29 ketone is much less efficient at the tip of the sepal. On the other hand, the mass spectra sampled from the middle of the sepal (Figure 3E; Table 1) indicates a very low abundance of epicuticular lipid molecules overall, suggesting that at the microscale this biosynthetic pathway is developmentally regulated through sepal development, so that epicuticular lipid accumulation increases as the sepal expands from its base. At this point, we want to point out that most sepal tissues sampled in Figure 2 were on the inner side of the sepal and inside the flower bud prior to flower opening (the outer side of the sepal was in contact with the sample plate and could not be sampled in these experiments). Our findings may indicate that the accumula-

(29) Nakata, Y.; Yamada, H.; Honda, Y.; Ninomiya, S.; Seki, T.; Aoki, T.; Matsuo, J. *Nucl. Instrum. Methods Phys. Res., Sect. B* **2009**, *267*, 2144.

(30) Samuels, L.; Kunst, L.; Jetter, R. *Annu. Rev. Plant Biol.* **2008**, *59*, 683–707.

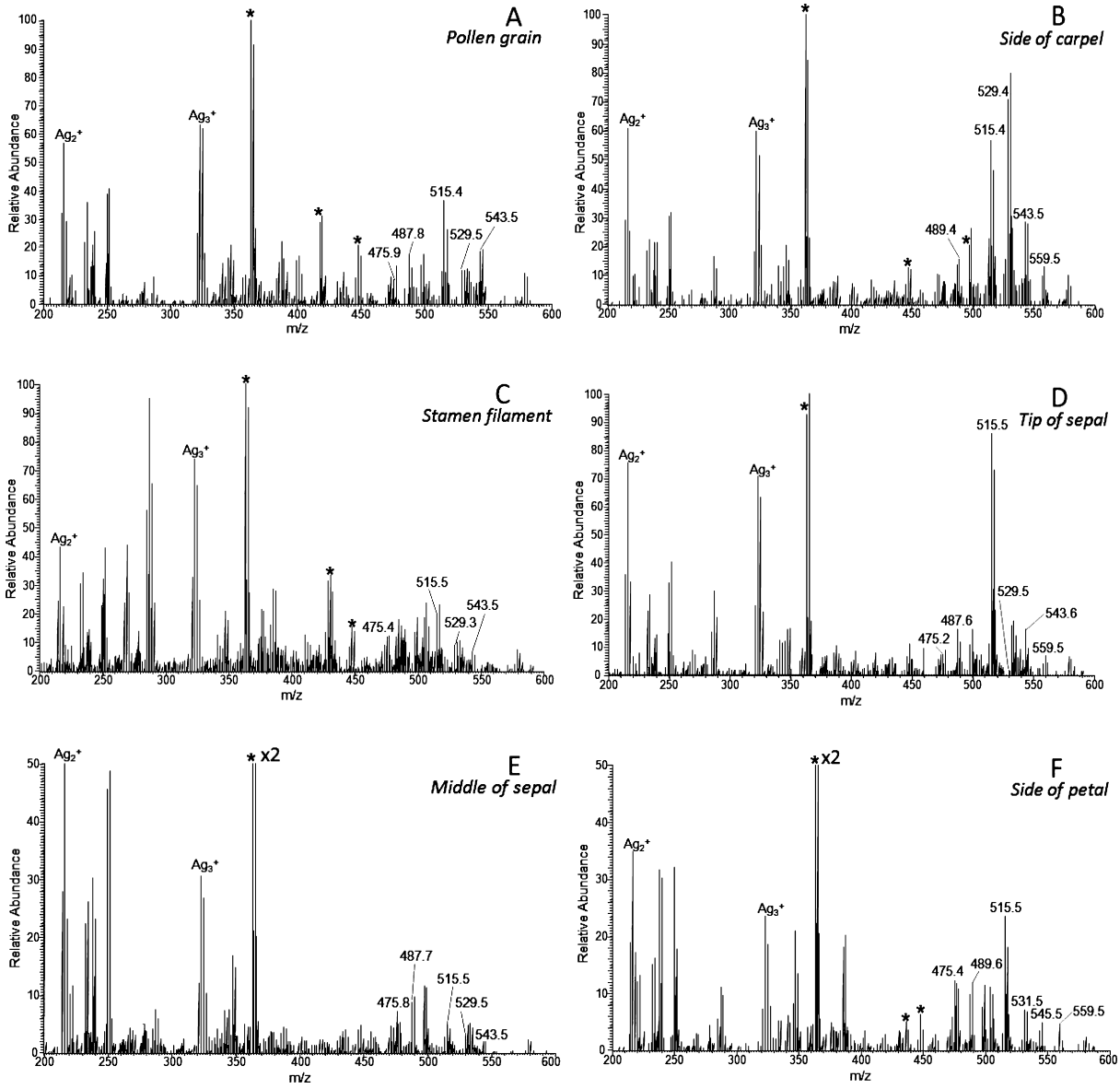

Figure 3. Single pixel mass spectra representing each part of flower tissues for the positions indicated in Figure 2: (A) pollen grain, (B) side of carpel, (C) stamen filament, (D) tip of sepal, (E) middle of sepal, (F) side of petal; * labeled peaks arise from contamination.

Table 1. Semiquantification of Surface Metabolites on Single Pixel of Flower Tissues[a]

		relative intensity (%)					
m/z	assignment	A pollen grain	B side of carpel	C stamen filament	D tip of sepal	E middle of sepal	F side of petal
487	[C27 alkane + ^{107}Ag]$^+$	25.2 ± 4.3	26.2 ± 5.6	28.3 ± 11.2	23.9 ± 4.2	19.4 ± 7.4	30.9 ± 16.9
515	[C29 alkane + ^{107}Ag]$^+$	66.6 ± 4.2	**99.8** ± 16.7	41.6 ± 3.0	**92.6** ± 20.0	25.2 ± 11.1	55.6 ± 17.7
543	[C31 alkane + ^{107}Ag]$^+$	35.0 ± 5.9	47.6 ± 7.6	13.2 ± 2.2	16.0 ± 5.7	9.2 ± 6.7	11.6 ± 3.8
491	[C26 alcohol + ^{109}Ag]$^+$	4.0 ± 2.3	6.4 ± 4.3	11.5 ± 8.0	3.8 ± 2.4	3.8 ± 2.5	3.0 ± 3.3
519	[C28 alcohol + ^{109}Ag]$^+$	8.5 ± 2.8	13.8 ± 2.7	7.7 ± 1.0	11.1 ± 3.0	6.2 ± 1.3	9.8 ± 3.6
547	[C30 alcohol + ^{109}Ag]$^+$	4.8 ± 3.8	**12.9** ± 4.7	2.5 ± 2.5	2.3 ± 0.5	1.2 ± 0.6	1.4 ± 0.8
475	[C24 fatty acid + ^{107}Ag]$^+$	13.8 ± 6.1	15.7 ± 6.3	23.0 ± 1.6	14.8 ± 2.2	13.6 ± 3.9	40.7 ± 24.0
503	[C26 fatty acid + ^{107}Ag]$^+$	12.8 ± 1.2	10.2 ± 0.4	26.7 ± 5.3	12.3 ± 4.2	6.7 ± 1.5	22.9 ± 6.1
559	[C30 fatty acid + ^{107}Ag]$^+$	2.0 ± 0.5	**19.4** ± 3.3	4.1 ± 1.7	7.9 ± 1.9	1.1 ± 0.7	12.7 ± 8.0
529	[C29 ketone + ^{107}Ag]$^+$	20.4 ± 2.7	**119.7** ± 16.1	11.1 ± 1.7	**5.6** ± 2.9	9.9 ± 7.1	8.8 ± 3.2

[a] Relative intensities are ion signals normalized to silver dimer, [^{107}Ag + ^{109}Ag]$^+$ (m/z 216). Standard deviation is obtained from multiple pixels near the positions indicated in Figure 2. Noticeable ion signals discussed in the text are marked in bold. C28 fatty acid is not included because the ^{107}Ag adduct (m/z 531) is overlapping with the isotopic contribution from C29 ketone, [C29 ketone + ^{107}Ag]$^+$, and the ^{109}Ag adduct (m/z 533) is overlapping with a matrix contaminant. ^{109}Ag adduct were used for alcohols because the m/z values of the ^{107}Ag adduct are overlapping with the ^{109}Ag adduct of alkanes.

tion of the epicuticular lipids is induced when the flower opens and these tissues are exposed to a drier environment, consistent with the water-barrier functionality of this material.[31] Therefore, the higher abundance of epicuticular lipids at the tip of sepal may be understood by the fact that the tip of sepal is partially exposed to air, to more desiccating conditions, and therefore there is a need for these lipids as a barrier to inhibit water-loss. The stamen filament and petal (C, F) have an average abundance level of epicuticular lipids compared to other flower tissues. We need to mention that the biochemical implication suggested above is our best speculation and subject to further verification; however, it is clear that our technology has revealed a new discovery of a high degree of localization of lipid metabolites which has not been previously possible and could lead to novel hypotheses. Previously, we compared the relative abundances of epicuticular lipid molecules on the surface of carpel, sepal, and petal but at a lower spatial resolution (~100 μm).[6] With the higher spatial resolution afforded by the modifications described herein, we could compare the distributions of these metabolites among fine locations in each tissue such as stamen filament, tip of sepal, and pollen grains (Table 1). The relative abundances of each lipid metabolite that were evaluated on a single pixel of carpel, sepal, and petal are similar to the data previously reported,[6] demonstrating the consistency of the method and the underlying biology.

In interpretation of the data generated via this method, there is a need for the careful consideration for the ionization efficiencies of the individual lipid metabolites and their changes on each tissue. In the discussion above, we made semiquantitative comparisons of the lipids on various parts of flower tissues, assuming that ion signals can be directly correlated with their abundances. Recently, Yost's group showed that matrix effects in MALDI ionization necessitate the need for internal standards for accurate quantification in MS imaging.[32] In fact, ion yields are subject to many variables, specifically, desorption efficiency, ionization efficiency, and instrument transmission efficiency. The last is relatively minor as they are typically mass dependent and the lipid molecules imaged in this study are within the narrow mass range of m/z 470−560.

The overall ionization efficiency could be quite different between each metabolite. For example, alkane ion signals are 10−100 times less than other epicuticular lipid molecules in LDI-MS according to in-parallel analyses conducted with GC/MS.[6] Although ion abundances of different lipid molecules cannot be directly compared to each other, the relative abundance of the same metabolite can be compared between different organs and tissues. Unlike typical MALDI, LDI with colloidal silver does not involve cocrystallization of the analytes with the matrix and it is unlikely that the adduct formation would incur at the same time with desorption process considering silver nanoparticles are sporadically scattered (Figure 1d). Hence, the ionization of epicuticular lipid metabolites as silver ion adducts seems to occur through a two step process, desorption from the surface and adduct formation in the gas phase. The latter would not be affected by the matrix because it occurs after desorption from the surface.

(31) Goodwin, S. M., Jenks, M. A. *Plant Abiotic Stress*; Jenks, M. A., Hasegawa, P. M., Eds.; Oxford: Oxford, U.K., 2005.

(32) Pirman, D. A.; Borum, P. R.; Yost, R. A. *Proceedings of the 57th ASMS Conference on Mass Spectrometry and Allied Topics*, Philadelphia, PA, May 31−June 4, 2009; poster session ThPF165.

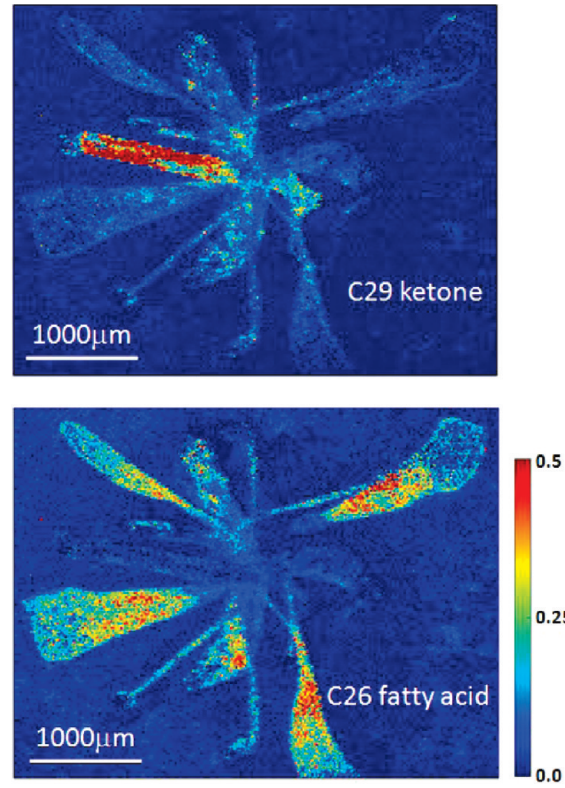

Figure 4. MS images of C29 ketone, [C29 ketone + ^{107}Ag]$^+$ (m/z 529), and C26 fatty acid, [C26 fatty acid + ^{107}Ag]$^+$ (m/z 503), normalized to the ion intensity of the silver dimer, [^{107}Ag + ^{109}Ag]$^+$ (m/z 216). The maximum color scales are 0.5 for both images for the same color scheme shown in Figure 2.

Desorption and ionization of the silver atoms could have a strong matrix effect, which in turn could affect silver ion adduct formation. This effect can be minimized by normalizing the ion current to the silver dimer peak. The former, desorption efficiency of each analyte, can also be affected by the matrix, but its effect is expected to be relatively small. Most plant surfaces consist of cuticles, and their van der Waals interaction with lipid molecules should not be significantly different among the tissues. With this hypothesis, the above discussion concerning the semiquantitative comparison of each metabolite between organs and tissues can thus be rationalized. We are planning to further confirm this hypothesis with known amounts of different internal standards sprayed on plant materials.

Figure 4 shows MS images of additional metabolites, specifically C29 ketone and C26 fatty acid. As noted in Figure 3 and Table 1, Figure 4 clearly demonstrates that C29 ketone is mostly concentrated on the carpel, while C26 fatty acid is dominant on the petal, stamen, and tip of the sepal. Figure 5A is a magnified image of the upper part of a stamen filament shown in Figure 2. Ion abundance profiles were taken along a series of single pixels vertically from the bottom of the image at the X position indicated by the arrow and for the Y coordinates between 2400 and 3000 μm from the base of the image (Figure 2). The constructed ion abundances for C29 alkane, C29 ketone, and C26 fatty acid are shown in Figure 5B. Periodic fluctuation of ion signals is quite noteworthy, typically one or two pixels of high abundance alternating with one of low abundance. This is probably an indication of cell-to-cell ion abundance variation that matches with

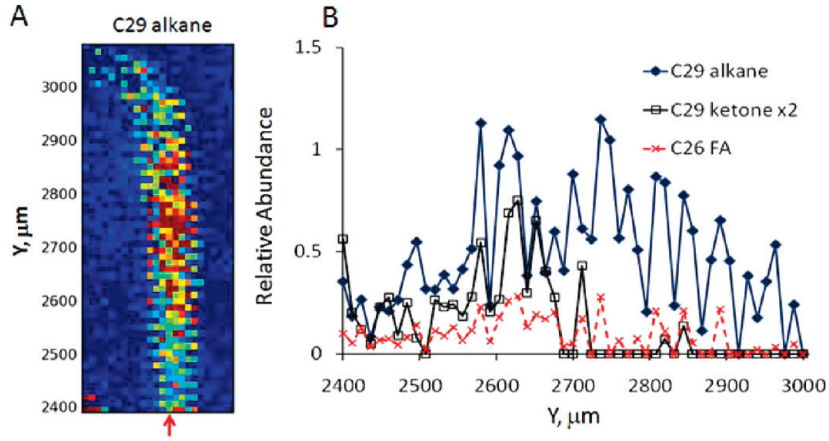

Figure 5. Single pixel profiles to demonstrate single cell level spatial resolution: (A) zoomed-in image of a stamen at the upper part of the flower shown in Figure 2; (B) relative ion abundance profiles for C29 alkane, C29 ketone, and C26 fatty acid as silver ion adducts (*m*/*z* 515, 529, and 503, respectively) normalized to the silver dimer, $[^{107}Ag\ +^{109}Ag]^+$ (*m*/*z* 216), along a series of single pixels vertically at the *X* position of 2100 μm indicated by the arrow in the left figure for *Y* positions of 2400−3000 μm from the base of the image in Figure 2. Periodic fluctuation of ion signals, typically every two or three pixels, matches with longitudinal epidermal cell size of ~30 μm on a stamen filament.

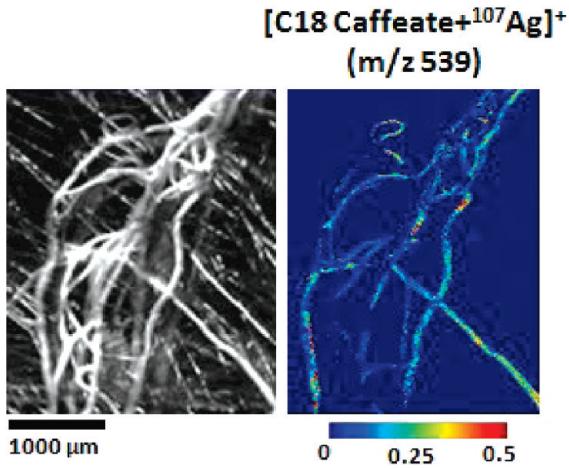

Figure 6. MS imaging of *Arabidopsis* root hairs: (left) optical image of *Arabidopsis* root and (right) MS image of silver ion adduct of C_{18} caffeate on an *Arabidopsis* root normalized to the silver dimer, $[^{107}Ag+^{109}Ag]^+$ (*m*/*z* 216), obtained with 12 μm spatial resolution.

the longitudinal epidermal cell size of ~30 μm along an *Arabidopsis* stamen filament.[33] Similar profiles could be obtained in a nearby series of pixels, as shown in Figure S-2 in the Supporting Information. The pixels with low ion signals may be aligned with the cell junctions and those with high ion signals may be from the center of epidermal cells. This is supporting evidence that the technology described herein has the capacity to image metabolites at a spatial resolution of approximating a single-cell.

High-Resolution MS Imaging of Roots. To further exploit this high spatial resolution technology, we applied MS imaging to *Arabidopsis* roots. Figure 6 shows the chemical image of C18 fatty alcohol caffeate ester, as a silver ion adduct, on an *Arabidopsis* root surface obtained with 12 μm spatial resolution. It shows fine chemical images of root structures. Submicrometer MS imaging of potassium and calcium has been performed on pine tree roots by Spengler and Hubert;[15] however, this is the first time MS imaging of secondary roots has been achieved for molecular species. We observed chemical compounds quite different from those of epicuticular lipid metabolites on other plant surfaces; examples include C18 fatty alcohol caffeate and C20 fatty alcohol coumarate esters. The high spatial resolution allowed us to study and image these metabolites directly on the root surface.

We encountered a number of difficulties specifically associated with imaging root samples, particularly during preparation of samples for MS imaging. Root samples are not flat and difficult to be attached flat to the surface, and therefore some parts of root fibers are not in the depth of field of the laser, resulting in not getting sufficient laser power for LDI. Thus, there is not enough ion signals in some local areas of Figure 6 to track the optical image. This implies that caution is needed in quantitative interpretation because the ion signals may be affected by the distorted laser depth of field and may not represent the actual amount of analyte present on the surface. We do not have this problem with other plant organs, such as flowers, leaves, or stems, which are more flexible and thin and can be easily attached to the plate flat.

It should be noted that the root image shown in Figure 6 is from the *cer*1 mutant of *Arabidopsis*. This image was acquired as a part of the experiment comparing MS images of surface metabolites between various plant tissues (flowers, leaves, stems, and roots)[34] of *cer*1 and wild type plants. Because *cer*1 has a mutation in the epicuticular lipid biosynthetic pathway, they show different abundances in epicuticular lipids, such as long chain alkanes, ketones, and fatty acids, as compared to the wild type (data not shown; manuscript in preparation). On the other hand, roots have different polymeric lipid structure, known as suberins. Unlike cuticles on the surfaces of aerial organs of plants, roots have different outer lipid metabolites, such as caffeate, coumarate, and ferulate esters. We could not observe any noticeable difference between MS images of these metabolites between wild type and the *cer1* mutant (wild type image not shown). These unusual lipid metabolites will be further discussed below together with accurate metabolite identification as confirmed with high-mass resolution data.

(33) Dinneny, J. R.; Weigel, D.; Yanofsky, M. F. *Development* **2006**, *133*, 1645–1655.

(34) Jun, J. H. L., Z. L.; Song, Z.; Nikolau, B. J.; Yeung, E. S.; Lee, Y. J. *Proceedings of the 57th ASMS Conference on Mass Spectrometry and Allied Topics*, Philadelphia, PA, May 31−June 4, 2009; oral session WOAam09:50.

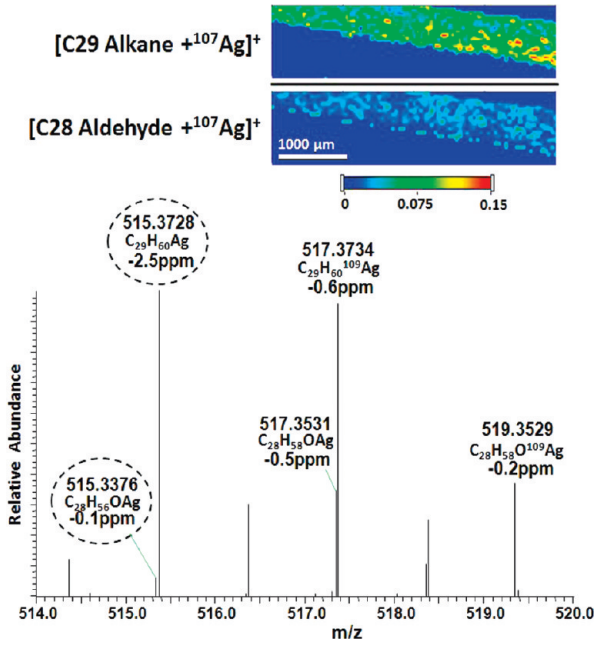

Figure 7. Differentiation of isobaric ions with high-resolution mass spectrometry: (top) MS images of silver ion adducts of C29 alkane (*m*/*z* 515.3728) and C28 aldehyde (*m*/*z* 515.3376) obtained on an *Arabidopsis* stem with MALDI LTQ-Orbitrap with 50 μm spatial resolution. Accurate mass imaging was constructed with mass tolerance of ±0.008 Da from their calculated masses. (Bottom) MALDI mass spectrum of an *Arabidopsis* stem shown for the *m*/*z* range 514−520 obtained with the MALDI LTQ-Orbitrap using colloidal silver as a matrix.

High Mass Resolution in MS Imaging. We adopted an LTQ Orbitrap with a MALDI source to acquire high-mass resolution spectra for metabolite imaging. The Discovery version of this instrument provides less mass resolution than other high-resolution mass spectrometers, 30 000 at *m*/*z* 400, but we could still routinely obtain mass accuracy of less than 3 ppm with internal calibration. The most important advantage of high mass resolution is differentiation of isobaric ions. A notorious example of isobaric ions that could not be distinguished previously in LDI-MS of plant metabolites was alkanes and aldehydes. Plant epicuticular aldehydes typically have even number of carbon atoms and alkanes have odd number of carbon atoms. The aldehyde functional group (CHO) has the same nominal mass as CH_2CH_3, or 29 Da (exact mass difference is 0.0364 Da), which results in aldehydes having the same nominal mass as the alkane homologue with one additional carbon atom. Figure 7 shows LDI-MS spectrum of epicuticular lipid metabolites on an *Arabidopsis* stem for the *m*/*z* range 514−520 obtained with the Orbitrap mass analyzer. ^{107}Ag adducts of C28 aldehyde and C29 alkane have the same nominal mass of *m*/*z* 515, but we can clearly differentiate the two metabolites in high-resolution MS. Chemical composition analysis exactly matches the experimental values within 3 ppm. These two lipid metabolites have almost no fragmentation in typical ion trap CID, so there are no good ways to differentiate these molecules other than high mass resolution. With high mass resolution, we can also construct separate MS images for C28 aldehyde and C29 alkane as shown in Figure 7.

In the mass spectrum shown in Figure 7, we can also differentiate the ^{109}Ag adduct of C29 alkane (*m*/*z* 517.3734) from the ^{107}Ag adduct of C28 alcohol (*m*/*z* 517.3531); both have a nominal mass of *m*/*z* 517 but have an exact mass difference of 0.0203 Da. In the previous report with the ion trap mass spectrometer,[6] the presence of C28 alcohol had been inferred from the GC/MS data and quantified with the ^{109}Ag adduct (*m*/*z* 519) in LDI-MS data, but high-resolution MS data clearly confirms its presence for both ^{107}Ag and ^{109}Ag adducts. Because of the unavailability of chromatographic separation in imaging MS, metabolomic profiling is often necessary in parallel to minimize but not eliminate false assignments. Therefore, high-resolution MS is extremely valuable to perform unambiguous identification of most metabolites directly from the sample surface without any separate analysis or prior knowledge of the sample. The MS/MS ability in the LTQ, of the LTQ-Orbitrap, can further assist the validation.

As mentioned above, we found unique lipid metabolites on the surface of roots that are quite different from typical epicuticular lipids on the surface of aerial organs. Li and co-workers performed GC/MS analysis of chloroform extracts of *Arabidopsis* roots and observed lipid compounds rich in C18−C22 alkyl esters of 4-hydroxycinnamic acids,[35] which we detected in MS imaging of root surfaces, e.g., C18 caffeate in Figure 6. MALDI LTQ-Orbitrap was used to characterize and/or confirm their identities on *Arabidopsis* root surfaces. As shown in Table 2, C18−C22 alkyl esters of coumarate, caffeate, and ferulate were found as major molecular species, as has been observed by Li and co-workers, together with a C29:2 sterol. The identification of these metabolites is based upon two criteria: (1) the match between their experimentally determined *m*/*z* values, which are within 3 ppm of theoretical predictions; and (2) GC/MS analysis of chloroform-extract of roots. The abundances determined by GC/MS analysis are mostly comparable to those by LDI LTQ-Orbitrap as shown in the Table 2. There are noticeable differences between sterols profiled by LDI-MS and GC/MS. GC/MS data, of both Li and co-workers' and ours, identified C28:1 and C29:1 sterols, while LDI-MS detected only C29:2 sterol. Considering that C28:1 and C29:1 sterols exist at much high abundance in GC/MS analysis and their ionization efficiencies must not be significantly different from that of C29:2 sterol, we suspect the difference might be due to the sampling depths between the two methods.

Other surface lipids found by Li and co-workers,[35] such as primary alcohols and fatty acids, were also detected in our GC/MS analysis (data not shown), but these were not detected by LDI-MS. There are two possible explanations for the absence of these surface lipids in LDI-MS imaging: (1) the shallow sampling depth in LDI-MS imaging as compared with chloroform extraction for GC/MS analysis and (2) low abundance of these lipid molecules on roots as compared with other organs; 10−100 times less abundant according to GC/MS analysis (data not shown).[6] One may consider low ionization efficiency could be another possible explanation, but it is unlikely considering we could detect those lipids on flowers (Table 1 and Cha et al.[6]), leaves (Cha et al.[6]), and stems (data not shown). It should be noted that there are a few days of unintentional gap in harvesting *Arabidopsis* roots between those used for GC/MS and LDI-MS; they are 16 and 21 days old, respectively, at the time of harvest. However, it would not affect the current result considering overall consistency in

(35) Li, Y. H.; Beisson, F.; Ohlrogge, J.; Pollard, M. *Plant Physiol.* **2007**, *144*, 1267–1277.

Table 2. Identification of Root Surface Metabolites Using the LTQ-Orbitrap[a]

		MALDI LTQ-Orbitrap			
		m/z			
ion species	chemical formula	experimental[b]	theoretical	relative intensity (%)[c]	wax load in GC/MS (nmol/g)[d]
[C28:1 sterol + ^{107}Ag]$^+$	$C_{28}H_{48}O^{107}Ag$	n.d.	507.2751		50.1 ± 9.1
[C29:1 sterol + ^{107}Ag]$^+$	$C_{29}H_{50}O^{107}Ag$	n.d.	521.2907		142.4 ± 3.0
[C29:2 sterol + ^{107}Ag]$^+$	$C_{29}H_{48}O^{107}Ag$	519.2736 ± 0.0015	519.2751	0.8 ± 0.4	21.6 ± 3.8
[C18 coumarate + ^{107}Ag]$^+$	$C_{27}H_{44}O_3{}^{107}Ag$	523.2335 ± 0.0001	523.2337	12.4 ± 9.3	87.2 ± 2.2
[C20 coumarate + ^{107}Ag]$^+$	$C_{29}H_{48}O_3{}^{107}Ag$	551.2648 ± 0.0001	551.2650	8.7 ± 5.0	47.3 ± 10.5
[C22 coumarate + ^{107}Ag]$^+$	$C_{31}H_{52}O_3{}^{107}Ag$	579.2961 ± 0.0002	579.2963	2.3 ± 1.1	10.0 ± 3.7
[C18 caffeate + ^{107}Ag]$^+$	$C_{27}H_{44}O_4{}^{107}Ag$	539.2285 ± 0.0003	539.2286	3.1 ± 3.2	3.4 ± 2.4
[C20 caffeate + ^{107}Ag]$^+$	$C_{29}H_{48}O_4{}^{107}Ag$	567.2596 ± 0.0005	567.2599	1.8 ± 1.8	0.7 ± 0.7
[C22 caffeate + ^{107}Ag]$^+$	$C_{31}H_{52}O_4{}^{107}Ag$	595.2911 ± 0.0004	595.2912	1.4 ± 0.9	0.09 ± 0.01
[C18 ferulate + ^{107}Ag]$^+$	$C_{28}H_{46}O_4{}^{107}Ag$	553.2450 ± 0.0014	553.2442	0.4 ± 0.2	2.7 ± 1.5
[C20 ferulate + ^{107}Ag]$^+$	$C_{30}H_{50}O_4{}^{107}Ag$	581.2768 ± 0.0011	581.2755	1.8 ± 0.5	1.1 ± 0.8
[C22 ferulate + ^{107}Ag]$^+$	$C_{32}H_{54}O_4{}^{107}Ag$	609.3056 ± 0.0010	609.3068	0.5 ± 0.6	0.1 ± 0.05

[a] Data from the *cer*1 mutant of *Arabidopsis thaliana* were shown. [b] Data were taken from a few representative pixels in root imaging obtained with 25 μm spatial resolution. n.d.: Not detected. [c] Relative intensities were obtained by normalizing ion intensities to the silver dimer, [^{107}Ag + ^{109}Ag]$^+$ (*m/z* 216). [d] Wax load is obtained from three replicates of GC/MS experiments.

GC/MS data between ours and Li and co-workers' in which 7 week-old roots were used.

The MALDI LTQ-Orbitrap system does not use an optical fiber for coupling the laser beam from the laser source to the mass spectrometer. Instead, the coupling was achieved through two mirrors and a lens.[27] Hence, we cannot use an optical fiber to narrow the laser beam diameter in this system and the inherent spot size with the N_2 laser is ~50 μm in its diameter. To achieve a smaller laser spot size, for higher spatial resolution, we placed a stainless steel plate with a pinhole with an aperture diameter of 3 mm in the laser beam path to mechanically reduce the beam size. This pinhole allowed us to achieve a laser spot size of ~25 μm, which does not provide precise images of roots as shown in Figure 6 but sufficient resolution to acquire high quality mass spectra for metabolite identifications as shown in Table 2 (image not shown).

Depth Resolved MS Imaging. Another challenge in MS imaging is to acquire chemical information in the third dimension, namely, depth. Caprioli and co-workers successfully demonstrated 3D MS imaging by acquiring 2D MS images from multiple layers of tissue slices prepared from a rat and a mouse brain.[36,37] In this study we attempted an alternative approach for acquiring depth profiling in submicrometer scales. Specifically, we adopted the concept of ion sputtering that is often used in surface analysis. In Auger electron spectroscopy or X-ray photoelectron spectroscopy, one sputters out the surface, layer by layer, with ion beams in order to obtain atomic concentrations as a function of depth. By analogy, one can envision that we could sputter out plant tissues, layer by layer, by using high-power laser beams to probe analytes at various depths.

To test the plausibility of this method, we performed the following preliminary experiment. We first acquired a 2D MS image of the surface metabolites of an *Arabidopsis* stem sprayed with colloidal graphite. Subsequently, we scanned the same surface area with multiple shots of the high-power laser. Before the next image acquisition, the sample plate was removed from the instrument for reapplication of the colloidal graphite matrix and reinserted into the mass spectrometer. Figure 8 shows MS images of a few example metabolites on the surface and deeper areas acquired before and after high-power laser sputtering of the same stem surface. Because colloidal graphite is not a good additive for ionizing nonpolar compounds, alkanes and ketones could not be detected in these analyses. However, a number of very-long chain fatty acids (C24−C30) were detected in high abundance on the surface of the stem, while kaempferol, a flavonoid, was not detected in this layer. In contrast, fatty acid metabolites were barely detectable in the deeper layer, while kaempferol was detected at much higher abundance. This distribution of these metabolites is consistent with our expectation that epicuticular lipid metabolites are present on the surface[6] and kaempferol and its derivatives are induced with exposure to higher light levels and they accumulate in the deeper layers of the plant tissue.[14] All the MS images were constructed in accurate mass from the data obtained with the Orbitrap, enhancing the confidence of their chemical assignments. By repeating the above procedure of laser sputtering, matrix application, and MS image-acquisition, we should be able to acquire MS images in multiple layers that can be used to generate 3D MS images of metabolites. More experiments need to be performed for samples with well-defined multilayers to further demonstrate the proof of concept.

There are a few obstacles that need to be overcome in this experimental approach. The significant bottleneck is the very long time required for data acquisition. Second, it is not clear whether the sputtering rate is homogeneous throughout the surface. Finally, there is a need to develop a means of calibrating the depth of each layer that is being examined.

CONCLUSIONS

We obtained a spatial resolution of ~12 μm in MS imaging by using an optical fiber with a 25 μm core diameter, and by improving matrix application through a modified oscillating capillary nebulizer device, and exploited it to obtain MS images of lipid metabolites on the surface of *Arabidopsis* flowers and roots. Single cell level MS imaging of a whole flower was achieved for the first time, which reveals fine features such as single pollen grains and enables comparisons of surface lipid metabolites from single pixel mass spectra on various plant tissues. The ion signals recorded

(36) Andersson, M.; Groseclose, M. R.; Deutch, A. Y.; Caprioli, R. M. *Nat. Methods* **2008**, *5*, 101–108.
(37) Crecelius, A. C.; Cornett, D. S.; Caprioli, R. M.; Williams, B.; Dawant, B. M.; Bodenheimer, B. *J. Am. Soc. Mass Spectrom.* **2005**, *16*, 1093–1099.

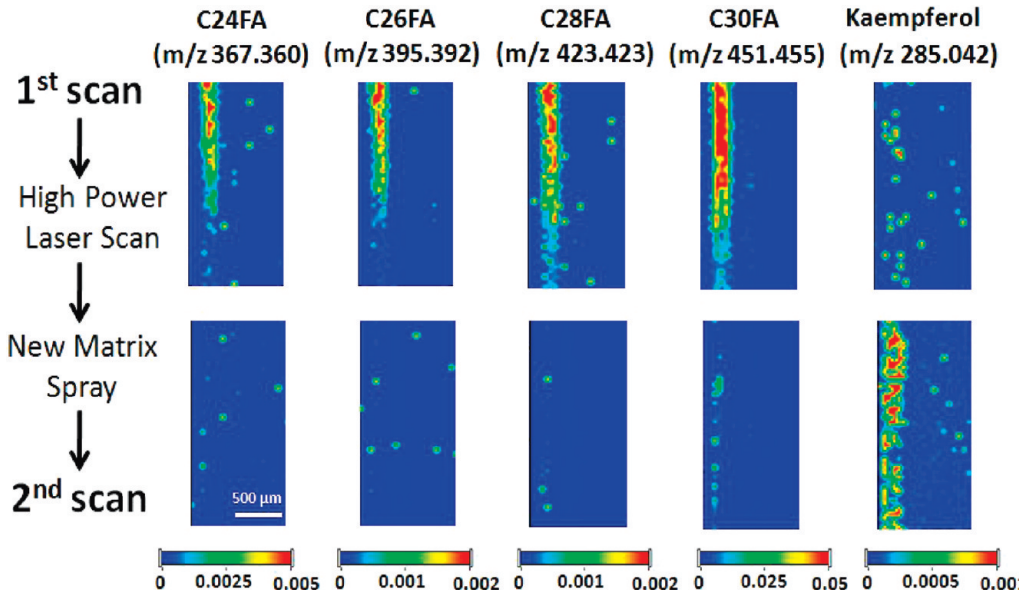

Figure 8. Depth profiling for MS imaging of *Arabidopsis* stem. MS images of C24−C30 fatty acids and kaempferol on an *Arabidopsis* stem obtained before (top row) and after (bottom row) surface sputtering with 480 laser shots at maximum laser power of 80 μJ/pulse. Colloidal graphite was used as a matrix, and MALDI LTQ-Orbitrap was used for data acquisition with 50 μm spatial resolution. The ion signals are normalized to total ion current (TIC).

here strongly suggest one should have enough signal even at a spatial resolution down to a few micrometers, offering the possibility of subcellular MS imaging. Ion abundance profiles along a series of single pixels on a stamen, for which the signal fluctuation matches the longitudinal epidermal cell size, supports our single cell level resolution. The capability of high mass resolution provided through the orbitrap mass analyzer was demonstrated in MS imaging of plant tissues. It made possible the differentiation of isobaric ions of aldehydes and alkanes and the direct identifications of surface metabolites on roots. The feasibility of 3D MS imaging is suggested through layer-by-layer surface sputtering by a laser beam.

Data acquisition time will become the most significant practical limitation in achieving MS imaging with both high spatial and high mass resolution. For example, it takes less than an hour to acquire an ion trap MS image of a whole *Arabidopsis* flower with a size of 4×3 mm^2 at 50 μm resolution but it takes 7−10 h at 12 μm resolution due to the larger number of pixels. For a spatial resolution of 5 μm, it will take over 40 h and it will take another 3−5 more times in the high-mass resolution mode. The last-mentioned experiments may be impossible due to the long-term instability of the laser beam and other experimental conditions. Imaging mass spectrometry in the microscope mode is suggested to be an alternative solution;[38] however, it suffers from the limited field of view. Further technical improvement is urgently needed to overcome this bottleneck, such as the recent development of a high speed time-of-flight mass spectrometer for MS imaging.[39]

(38) Luxembourg, S. L.; Mize, T. H.; McDonnell, L. A.; Heeren, R. M. *Anal. Chem.* **2004**, *76*, 5339–5344.
(39) Vestal, M.; Hayden, K. *Int. J. Mass Spectrom.* **2007**, *268*, 83–92.

ACKNOWLEDGMENT

The authors thank Sangwon Cha for his technical advice and James W. Anderegg in the Ames Laboratory for the SEM images. We also acknowledge the technical expertise and advice of Ann Perera, W. M. Keck Metabolomics Research Laboratory. The Ames Laboratory is operated for the U.S. Department of Energy by Iowa State University under Contract No. DE-AC02-07CH11358. This work was supported by U.S. Department of Energy, Office of Basic Energy Science, Division of Chemical Sciences.

SUPPORTING INFORMATION AVAILABLE

Additional information as noted in text. This material is available free of charge via the Internet at http://pubs.acs.org.

Received for review December 31, 2009. Accepted March 5, 2010.

AC902990P